# Iodide-CIMS and *m/z* 62: The detection of $HNO_3$ as $NO_3^-$ in the presence of PAN, peroxyacetic acid and ozone

Raphael Dörich,[1] Philipp Eger,[1] Jos Lelieveld[1] and John N. Crowley.[1]

[1]Atmospheric Chemistry Department, Max Planck Institute for Chemistry, 55128, Mainz, Germany

*Correspondence to*: John N. Crowley (john.crowley@mpic.de)

**Abstract.** Chemical Ionisation Mass Spectrometry (CIMS) using $I^-$ (the iodide anion) as primary reactant ion has previously been used to measure $NO_3$ and $N_2O_5$ both in laboratory and field experiments. We show that reports of the large daytime mixing ratios of $NO_3$ and $N_2O_5$ (both usually present in detectable amounts only at night) are likely to be heavily biased by the ubiquitous presence of $HNO_3$ in the troposphere and lower stratosphere. We demonstrate in a series of laboratory experiments that the CIMS detection of $HNO_3$ at *m/z* 62 using $I^-$ ions is efficient in the presence of peroxy acetyl nitric anhydride (PAN) or peroxyacetic acid (PAA) and especially $O_3$. We have characterised the dependence of the sensitivity to $HNO_3$ detection on the presence of acetate anions ($CH_3CO_2^-$, *m/z* 59, from either PAN or PAA). The loss of $CH_3CO_2^-$ via conversion to $NO_3^-$ in the presence of $HNO_3$ may represent a significant bias in I-CIMS measurements of PAN and PAA in which continuous calibration (e.g. via addition of isotopically labelled PAN) is not carried out. The greatest sensitivity to $HNO_3$ at *m/z* 62 is achieved in the presence of ambient levels of $O_3$ whereby the thermodynamically disfavoured, direct reaction of $I^-$ with $HNO_3$ to form $NO_3^-$ is bypassed by the formation of $IO_X^-$, which react with $HNO_3$ to form e.g. iodic acid and $NO_3^-$. The ozone and humidity dependence of the detection of $HNO_3$ at *m/z* 62 was characterised in laboratory experiments and applied to daytime, airborne measurements in which good agreement with measurements of the $I^-(HNO_3)$ cluster-ion (specific for $HNO_3$ detection) was obtained. At high ozone mixing ratios, we show that the concentration of $I^-$ ions in our IMR is significantly depleted. This is not reflected by changes in the measured $I^-$ signal at *m/z* 127 as the $IO_X^-$ formed do not survive passage through the instrument, but are likely detected after fragmentation to $I^-$. This may result in a bias in measurements of trace gases using I-CIMS in stratospheric air masses unless a calibration gas is continuously added or the impact of $O_3$ on sensitivity is characterised.

## 1 Introduction

The use of iodide anions ($I^-$) as primary ions in mass-spectrometric studies of ion-molecule reactions has a long history. Fehsenfeld et al. (1975) and Davidson et al. (1978) established that the nitrate anion ($NO_3^-$, *m/z* 62) was formed in a rapid reaction between $I^-$ and $N_2O_5$. $NO_3^-$ was also identified as the main product of the reaction between $I^-$ and $ClONO_2$ (Huey et al., 1995). The large rate constants for reaction of $I^-$ with $N_2O_5$ and $ClONO_2$ led to the development of Chemical Ionisation Mass Spectrometry (CIMS) using $I^-$ primary ions (henceforth I-CIMS) in kinetic studies of heterogeneous, atmospheric

reactions (e.g. (Hanson and Ravishankara, 1991)) and more recently has found widespread deployment for measurement of atmospheric trace gases ((Huey (2007) and references therein). Early field measurements utilised I-CIMS to detect $N_2O_5$ and peroxyacetyl nitric anhydride (PAN, $CH_3C(O)O_2NO_2$) (Slusher et al., 2004) but since then the range of molecules that have been detected using $I^-$ has greatly increased and trace-gases as diverse as inorganic radicals and halogenates and a host of

35    organic species are now routinely measured (Huey, 2007; Lee et al., 2014; Iyer et al., 2017; Riva et al., 2019). In this work, we focus on the detection of two atmospherically important trace gases $N_2O_5$ and $HNO_3$ using a CIMS operating with $I^-$ reactant ions.

Both $N_2O_5$ and $HNO_3$ are formed in the atmosphere by the sequential oxidation of NO, which has both anthropogenic and natural sources. In a well-known series of reactions (Lightfoot et al., 1992; Atkinson et al., 2004), NO is oxidised (R1, R2)

40    by reaction with $O_3$ or peroxyl radicals ($RO_2$) to $NO_2$, which during the day, may be removed by reaction with OH to form $HNO_3$ (R3) and during the night to form $N_2O_5$ (R4, R5).

| | | | |
|---|---|---|---|
| $NO + O_3$ | $\rightarrow$ | $NO_2 + O_2$ | (R1) |
| $NO + RO_2$ | $\rightarrow$ | $NO_2 + O_2$ | (R2) |
| $NO_2 + OH + M$ | $\rightarrow$ | $HNO_3 + M$ | (R3) |
| 45    $NO_2 + O_3$ | $\rightarrow$ | $NO_3 + O_2$ | (R4) |
| $NO_3 + NO_2 + M$ | $\rightarrow$ | $N_2O_5 + M$ | (R5) |

Both $HNO_3$ and $N_2O_5$ have important, non-gas-phase loss processes (Crowley et al., 2010) such as uptake to particles and other surfaces. In addition, $N_2O_5$ can thermally dissociate back to $NO_3$.

The chain of reactions to form $N_2O_5$ is broken during the day as $NO_3$ is generally photolysed within a few seconds (Wayne et

50    al., 1991) and also reacts with NO so that $N_2O_5$ is expected to be present at significant levels only at night-time.

The detection of $N_2O_5$ using $I^-$ reactant ions can be achieved by monitoring either the $NO_3^-$ product at $m/z$ 62 (see above) or the adduct ion at $m/z$ 235 (Kercher et al., 2009). The former is reported to be more sensitive and less dependent on water vapour concentrations but less specific, with large and highly variable background signals potentially arising from trace gases such as $NO_3$, $ClONO_2$ and $BrONO_2$. Despite this, night time $N_2O_5$ has been monitored in ambient air (as $NO_3^-$) using $I^-$

55    reactant ions, showing reasonable agreement with optical methods (Slusher et al., 2004; Dubé et al., 2006; Chang et al., 2011).

During a recent, airborne deployment of our I-CIMS, we monitored $NO_3^-$ at $m/z$ 62 in an attempt to detect $N_2O_5$ during two night-time flights. The air masses we investigated were mainly in the tropical free and upper troposphere and lower stratosphere and we did not expect significant interference from e.g. halogen nitrates at $m/z$ 62. However, our airborne

60    measurements (described in detail in section 4) revealed a large and variable signal at $m/z$ 62 during both the day and night. To illustrate this, raw signals obtained during daytime when the aircraft sampled air masses with varying degrees of stratospheric influence are displayed in Fig. S1. The signal at $m/z$ 62 is large and highly variable and is not affected by addition of NO to the heated inlet, ruling out its assignment to either $N_2O_5$ or $NO_3$ (see below). The great increase in signal

when entering the lower stratosphere and the obvious correlation with $O_3$ (Fischer et al., 1997; Popp et al., 2009) provided an early clue to the identity of the trace-gas detected at $m/z$ 62 which we initially assigned to $HNO_3$. Our results thus appeared to contrast the conclusions of a previous observation of a large daytime signal at $m/z$ 62 when deploying an I-CIMS (in this case in the boundary layer), which was interpreted as resulting (at least in part) from high levels of daytime $NO_3$ and/or $N_2O_5$ (Wang et al., 2014). Based on complementary laboratory experiments, Wang et al. (2014) showed, in accord with earlier investigations (Fehsenfeld et al., 1975; Huey et al., 1995), that $HNO_3$ is not detected sensitively at $m/z$ 62 using I-CIMS.

The unexpected observation of a large daytime signal at $m/z$ 62 during airborne operation led us to perform a series of laboratory experiments to identify potential "interfering" trace gases at this mass-to-charge ratio when using I-CIMS. In contrast to the conclusions drawn from previous studies, our laboratory and airborne measurements show that, during daytime, the predominant contributor to $m/z$ 62 when sampling ambient air (in the presence of ozone) is likely to be $HNO_3$.

## 2 Experimental details

The I-CIMS we used in our laboratory and airborne investigations (see Fig. 1) is similar to that described by Slusher et al. (2004) and Zheng et al. (2011) and was originally constructed in collaboration with Georgia Tech as a prototype instrument of the company THS (http://thsinstruments.com). It is essentially a hybrid of the instruments described by Phillips et al. (2013) and Eger et al. (2019), the former using a $^{210}$Po ion source, the latter an electrical discharge source but with improved (digital) control of the MS settings enabling different mass-to-charge ratios to be monitored using different potentials for the collisional dissociation of cluster ions. For all the experiments described below, the $^{210}$Po ion source was used to generate $I^-$ as this configuration has much better sensitivity for PAN, the main target trace gas during the deployment of the I-CIMS on the HALO aircraft (High Altitude Long range platform for atmospheric Observations). The set-up for PAN detection includes a heated inlet section (~170 °C, 100 mbar, residence time ~ 40 ms) to thermally dissociate PAN to $CH_3C(O)O_2$ which subsequently reacts with $I^-$ to form the acetate anion ($CH_3CO_2^-$) which is detected at $m/z$ 59. At this inlet temperature and pressure, the lifetime of PAN with respect to thermal decomposition < 3 ms (IUPAC, 2021). For $N_2O_5$, the lifetime with respect to its thermal dissociation to $NO_2$ and $NO_3$ is ~0.5 ms (IUPAC, 2021)) so that $N_2O_5$ is stoichiometrically converted to $NO_3$ and the instrument measures the sum of $N_2O_5$ and $NO_3$ at $m/z$ 62. In order to separate PAN signals from those of peroxyacetic acid ($CH_3C(O)OOH$, also detected as $CH_3CO_2^-$ at $m/z$ 59) we periodically add NO (~ $5 \times 10^{12}$ molecule cm$^{-3}$) to the inlet to remove $CH_3C(O)O_2$ and thus eliminate sensitivity to PAN. As NO reacts more rapidly with $NO_3$ than with $CH_3C(O)O_2$ at 170 °C ($k_{NO+NO3} = 2.3 \times 10^{-11}$ cm$^3$ molecule$^{-1}$ s$^{-1}$ , $k_{NO+CH3C(O)O2} = 1.4 \times 10^{-11}$ cm$^3$ molecule$^{-1}$ s$^{-1}$ (IUPAC, 2021)) the concentration of NO added is also sufficient to quantitatively titrate $NO_3$ to $NO_2$ and thus provides a measure of the "background" signal at $m/z$ 62 in the absence of $NO_3$ and $N_2O_5$.

During airborne operation on HALO, the dynamic pressure generated in a forward facing trace gas inlet (TGI) located on top of the aircraft (see Fig. 1) was used to create a flow of air through ¼ inch (OD) PFA tubing sampling at an angle of 90° to the flight direction. The ¼ inch tubing was attached to a ½ inch (OD) PFA tube attached to an exhaust plate at the underside

of the aircraft to create a fast "bypass" flow. The bypass flow was sub-sampled (again at 90° and by ¼ inch PFA tubing heated to 40°C) by the 1.4 L (STP) min$^{-1}$ flow into the I-CIMS. Sub-sampling twice at 90° to the flow was helpful in reducing the number of large particles (e.g. cloud droplets) that could enter the thermal dissociation inlet and IMR.

The thermal dissociation inlet of the I-CIMS is regulated to a pressure of 100 mbar, which results in a pressure in the ion-molecule reactor of 24 mbar. This way, a stable pressure in the thermal dissociation inlet and the Ion Molecule Reactor (IMR) was maintained at altitudes up to ~15 km. Prior to take off, the inlet line and TGI were flushed with nitrogen to prevent contamination by the high levels of pollutant trace gases at the airport. As described in Eger et al. (2019) negative ions exiting the IMR were declustered in passage through a collisional dissociation region (CDC, 0.6 mbar) before passing through an octopole ion-guide ($6 \times 10^{-3}$ mbar) and a quadrupole for mass selection ($9 \times 10^{-5}$ mbar) prior to detection using a channeltron.

$I^-$ ions were generated by combining flows of 4 cm$^3$ (STP) min$^{-1}$ CH$_3$I/N$_2$ (400 ppmv) with 750 cm$^3$ (STP) min$^{-1}$ N$_2$ and passing the mixture through a 370 MBq $^{210}$Po source. Under standard operating conditions (including airborne deployment), a constant amount of H$_2$O was added to the IMR by flowing 50 cm$^3$ (STP) min$^{-1}$ N$_2$ (at 1 bar pressure) through a 30 cm length of water-permeable 1/8-inch tubing (Permapure) immersed in water. The 50 cm$^3$ (STP) min$^{-1}$ flow of N$_2$ acquires a relative humidity close to 100 % in transit through the tubing and is subsequently mixed with the dry N$_2$ flow and sample air. Under these conditions, the ratio of signals at $m/z$ 145 ($I^-(H_2O)$) to that at $m/z$ 127 ($I^-$) was 0.068. By comparison with calibration curves (see Fig S2 and associated text) this indicates an H$_2$O concentration in the IMR of ~$4 \times 10^{14}$ molecule cm$^{-3}$. For laboratory tests, the amount of water in the IMR could be increased by reducing the pressure in the permeable tube (thus increasing the mole fraction of H$_2$O) or set to zero by bypassing the humidifier.

Based on a (calculated) literature value for the free energy of formation of $I^-(H_2O)_1$ of -6.1 kcal mol$^{-1}$ (Teiwes et al., 2019) we derive an equilibrium constant (at 298 K) of $K_6 = 1.16 \times 10^{-15}$ cm$^3$ molecule$^{-1}$ for the formation and thermal dissociation of $I^-(H_2O)_1$

$$I^- + H_2O \quad\rightleftharpoons\quad I^-(H_2O)_1 \hspace{6cm} (R6)$$

With an H$_2$O concentration (in the IMR) of $3.9 \times 10^{14}$ molecule cm$^{-3}$ this implies that the ratio [$I^-(H_2O)_1$] / [$I^-$] = 0.45. Our measured ratio of signals at $m/z$ 145 ($I^-(H_2O)$) / $m/z$ 127 ($I^-$) was a factor ~6 lower, reflecting the fact that, even when the declustering potential is reduced to its minimum value, most $I^-(H_2O)$ ions do not survive the CDC region.

During extended operation of the CIMS, changes in sensitivity were captured by monitoring the primary ion signal ($I^-$ and its water cluster). Background signals at each of the mass-to-charge ratios monitored were obtained by passing the sampled air through a tubular scrubber (aluminium) filled with stainless-steel wool heated to 120 °C.

 **3 Laboratory Characterisation**

**3.1 Detection of HNO₃ at *m/z* 62: The role of ozone**

As described above, our observations of a clear correlation between *m/z* 62 and $O_3$ mixing ratios during the first HALO deployment of the I-CIMS strongly suggested that $HNO_3$ was the origin of the signal although previous experiments had shown that $I^-$ does not react with $HNO_3$ to form $NO_3^-$. In order to determine the sensitivity of our I-CIMS to $HNO_3$ we constructed a permeation source in which a 20 cm³ (STP) min⁻¹ flow of zero air was passed through a 1m length of PFA tubing (0.125 inch OD) which was formed into a coil and submerged in an aqueous solution of 65% $HNO_3$ held at 50°C. The permeation rate was determined by passing the 20 cm³ (STP) min⁻¹ flow through an optical absorption cell and measuring the optical extinction at 185 nm where the absorption cross-section of $HNO_3$ is well known (Dulitz et al., 2018). For the I-CIMS calibration, the 20 cm³ (STP) min⁻¹ output was dynamically diluted to generate a mixing ratio of between 5 and 50 ppbv. Based on uncertainties in the absorption cross-section (5%), the reproducibility of the optical measurement and the dilution factor, the uncertainty of the $HNO_3$ mixing ratio is estimated as 15 %.

Figure 2 shows the response of the I-CIMS at *m/z* 62 to addition of various amounts of $HNO_3$. Throughout the paper, when presenting raw data, we generally normalise the I-CIMS signal by dividing by the primary ion signal at *m/z* 127. This is standard practise and corrects for drifts in the $CH_3I$ flow which may occur over several hours after the instrument was switched from standby mode to operational mode. It also accounts for longer-term drifts caused by the weakening activity of the [210]Po source over the duration of a measurement campaign (months) or since the last calibration and for loss of detector sensitivity over similar time periods. We show later that, when adding large concentrations of reactants that significantly deplete the primary ion signal at *m/z* 127, this procedure may lead to bias is some measurements. For this reason, when detecting $HNO_3$ at *m/z* 190 (see later), we normalise to an interpolated signal at *m/z* 127 that was measured when the air was scrubbed.

The weak signal in the absence of $O_3$ (blue data points) confirms the conclusions of previous studies that derive a low rate coefficient for reaction (R7). For comparison, approximate, relative sensitivities to PAN (*m/z* 59), $N_2O_5$ (*m/z* 62) and $HNO_3$ (*m/z* 62), using this instrument are 1, 0.1 and $5 \times 10^{-4}$, respectively. Indeed, as written below, reaction (R7) is endothermic by ~43 kJ mol⁻¹ (Goos et al., 2005).

$I^-$ + $HNO_3$ $\rightarrow$ $NO_3^-$ + HI (R7)

In a further series of experiments, we measured the response of the I-CIMS to $HNO_3$ when adding $O_3$ to the zero-air. The results, also plotted in Fig. 2 (black symbols), indicate a factor ~250 increase in the signal at *m/z* 62 when ~500 ppbv ozone was added. There are two possible explanations for this observation. The first involves conversion of $NO_2$ impurity (that is present as a ~8 % impurity in the $HNO_3$ permeation flow) to $NO_3$ and $N_2O_5$ (R1, R4, R5) which are subsequently detected. This can however be ruled out as the rate-limiting step in the formation of $NO_3$ is the slow reaction between $NO_2$ and $O_3$ with $k_4 = 3.5 \times 10^{-17}$ cm³ molecule⁻¹ s⁻¹ at room temperature (Atkinson et al., 2004). The addition of 1000 ppbv $O_3$ (equivalent to a concentration of $2.4 \times 10^{13}$ molecule cm⁻³) would only convert an insignificant fraction of the $NO_2$ to $NO_3$ in

the ~40 ms reaction time available from the point of mixing to the IMR. This was confirmed by adding NO (7.7 ppm) to the inlet which would remove any $NO_3$ (see above) and observing no change in the signal at $m/z$ 62.

160    The second explanation is that the presence of $O_3$ results in the generation of further reagent ions that can react with $HNO_3$. Iodide anions are known to react with $O_3$, leading, in a series of exothermic reactions, to the formation of iodate (Williams et al., 2002; Teiwes et al., 2018; Bhujel et al., 2020).

$$I^- + O_3 \quad\quad \rightarrow \quad\quad IO^- + O_2 \quad\quad\quad\quad\quad\quad\quad\quad\quad\quad\quad\quad\quad (R8)$$

$$IO^- + O_3 \quad\quad \rightarrow \quad\quad IO_2^- + O_2 \quad\quad\quad\quad\quad\quad\quad\quad\quad\quad\quad\quad\quad (R9)$$

165    $$IO_2^- + O_3 \quad\quad \rightarrow \quad\quad IO_3^- + O_2 \quad\quad\quad\quad\quad\quad\quad\quad\quad\quad\quad\quad\quad (R10)$$

In this scheme, R8 is rate-limiting ($k_8$ ~$1 \times 10^{-12}$ $cm^3$ molecule$^{-1}$ s$^{-1}$ (Bhujel et al., 2020), whereas the further steps (R9-R10) in the sequential oxidation to iodate proceed with rate constants at least two orders of magnitude larger (Teiwes et al., 2018; Bhujel et al., 2020). $IO^-$ and $IO_2^-$ also react with $O_2$ to reform $O_3$:

$$IO^- + O_2 \quad\quad \rightarrow \quad\quad I^- + O_3 \quad\quad\quad\quad\quad\quad\quad\quad\quad\quad\quad\quad\quad (R11)$$

170    $$IO_2^- + O_2 \quad\quad \rightarrow \quad\quad IO^- + O_3 \quad\quad\quad\quad\quad\quad\quad\quad\quad\quad\quad\quad\quad (R12)$$

with rate coefficients of $k_{11} = 3.2 \times 10^{-14}$ $cm^3$ molecule$^{-1}$ s$^{-1}$ and $k_{12} = 1.3 \times 10^{-14}$ $cm^3$ molecule$^{-1}$ s$^{-1}$ (Bhujel et al., 2020). With the $O_3$ (~$1$-$5 \times 10^{10}$ molecule $cm^{-3}$), $O_2$ concentrations (~ $4 \times$ that of $O_3$) and reaction times used in their studies (Teiwes et al., 2018; Teiwes et al., 2019; Bhujel et al., 2020) $IO_3^-$ was observed to be the dominant form of $IO_X^-$.

In the presence of water vapour, $I^-$ is also present as a hydrate $I^-(H_2O)$ (see above) for which, according to Teiwes et al. 175    (2019), the rate coefficient for reaction with $O_3$ (R13a, R13b) is a factor ~40 larger than $k_8$ and results in the formation of $IO_2^-$ and $I^-$ :

$$I^-(H_2O) + O_3 \quad\quad \rightarrow \quad\quad IO_2^- + \text{neutrals} \quad\quad\quad\quad\quad\quad\quad\quad\quad\quad\quad (R13a)$$

$$I^-(H_2O) + O_3 \quad\quad \rightarrow \quad\quad I^- + \text{neutrals} \quad\quad\quad\quad\quad\quad\quad\quad\quad\quad\quad\quad (R13b)$$

As R8 is rate limiting, this implies an increase in the amount of e.g. $IO_3^-$ formed in the IMR in the presence of water. In most 180    regions of the troposphere and lower atmosphere ozone mixing ratios lie between 30 and >1000 ppbv. An ambient ozone concentration of 50 ppbv results in a concentration in the IMR of > $10^{10}$ molecules $cm^{-3}$. The large rate coefficients for R9 and R10 and the reactions of $IO^-$ and $IO_2^-$ with $O_2$ result in the rapid inter-conversion of $I^-$, $IO^-$, $IO_2^-$ and $IO_3^-$ which results (for a given RH and ozone concentration) in a quasi-equilibrium between $IO_X^-$ anions.

We explored the relevance of these reactions for our I-CIMS by carrying out a set of experiments in which varying amounts 185    of $O_3$ were added to the inlet and the mass-to-charge ratios corresponding to $IO^-$ ($m/z$ 143), $IO_2^-$ ($m/z$ 159) and $IO_3^-$ ($m/z$ 175) were monitored; the results are depicted in Fig. 3.

First, we note that all three mass-to-charge ratios were indeed observed, but only under conditions where the CDC potential was set to the lowest value at which ions still reach the detector. The dependence of the various $IO_X^-$ anions on the $O_3$ mixing ratio is broadly as expected from the reaction scheme (R8-R12) listed above: The major contributor to $IO_X^-$ at low [$O_3$] is $IO^-$, 190    which is converted to $IO_2^-$ and $IO_3^-$ more efficiently as $O_3$ increases, while the total concentration of $IO_X^-$ increases

approximately linearly. At the maximum $O_3$ mixing ratio used (577 ppbv) there are (following dilution) 375 ppbv in the IMR, which translates to a concentration (at 24 mbar and ~298 K) of $2.1 \times 10^{11}$ molecule $cm^{-3}$. This $O_3$ concentration is comparable with those used by Teiwes et al. (2018) (~1-4 $10^{11}$ molecule $cm^{-3}$) or Bhujel et al. (2020) (~$4 \times 10^{10}$ molecule $cm^{-3}$) in their ion-trap based, kinetic investigations of the formation of $IO_X^-$ when reacting $I^-$ with $O_3$. Their observation that

195   $IO_3^-$ is the dominant anion is however not consistent with our results, which indicate that $IO_3^-$ represents only ~35% of the total $IO_X^-$ signal. The relative abundance of each $IO_X^-$ depends not only on the $O_3$ concentration but also on the reaction time, which, for both Teiwes et al. (2018) and Bhujel et al. (2020) was between 10-100 ms. Based on the flow into the IMR, its volume (~50 $cm^3$) and the pressure we calculate a similar residence time (for neutrals) of about 25 ms. We also considered the possibility that the application in our I-CIMS of a potential difference between the entrance and exit of the IMR (to

200   optimise ion-transmission) could result in a significantly shorter IMR-residence time for ions. This was assessed by calculating the drift-velocity ($V_d$) in the IMR from the electric field strength ($E$ ~12 $Vm^{-1}$) and the ion mobility ($\mu$).

$$V_d = E\mu \tag{1}$$

The electrical mobility of $I^-$ was calculated for our conditions (using the Mason-Schamp equation) as ~ 0.15 $m^2\,V^{-1}\,s^{-1}$ using a collision cross-section (for an $I^-$ / $N_2$ pair) of $9 \times 10^{-16}$ $cm^2$ $molecule^{-1}$ (McCracken, 1952). Via equation (1), this results in a

205   drift velocity of 1.8 m $s^{-1}$, or an ion residence time (in the ~8 cm long IMR) of 44 ms, which is comparable to the residence time of neutrals. Note that the IMR reaction times we derive are only approximate as we do not take into account the mixing and flow dynamics in the IMR, which are likely to be complex (and possibly shorter than 25 ms) owing to sampling via a critical orifice. While we cannot rule out that our observation of $IO^-$ (and not $IO_3^-$) being the dominant ion-signal is partially caused by differences in reaction times, slight differences in $O_3$ concentrations and differences in temperature (our IMR is at

210   ~15°C above ambient temperature owing to the heated inlet) we note that the higher pressure of $O_2$ (factor ~1-10 $\times 10^4$) in our IMR is likely to have a large effect. The presence of $O_2$ converts $IO_3^-$ back to $IO^-$ thus competing with further oxidation (via reaction with $O_3$) to $IO_3^-$. Additionally, the high IMR pressures (24 mbar) in our experiments are ~ six orders of magnitude higher than the ~$10^{-5}$ mbar available in the ion-trap experiments of Teiwes et al. (2018) and Bhujel et al. (2020) which will result in more rapid thermalization of the ions present and prevent potentially non-thermal reactions and thus bias

215   to the rate coefficients derived.

The effect of adding $H_2O$ to the IMR was explored in a further set of experiments and the variation of the signals at mass-to-charge ratios corresponding to $IO_X^-$ with [$H_2O$] are displayed in Fig. 4. The experiments were carried out with the $O_3$ mixing ratio fixed at either 70 or 120 ppbv, close to that typically found in the lower troposphere (~20-100 ppbv). At the lowest $H_2O$ concentrations in our experiments, the total $IO_X^-$ signal is about 30 counts. This increases by a factor of ~10 when [$H_2O$]$_{IMR}$

220   increases to $3 \times 10^{15}$ molecule $cm^{-3}$. Increasing the $O_3$ mixing ratio from 70 to 120 ppbv results in an increase in the signals at $m/z$ 175 ($IO_3^-$) and $m/z$ 159 ($IO_2^-$) at all water vapour concentrations, whereas the signal at $m/z$ 143 ($IO^-$) is reduced at the lowest water vapour concentrations. These observations reinforce the concept of a larger rate coefficient for reaction of

I⁻(H₂O) with O₃ (R13a) compared to I⁻ (R8) (Teiwes et al., 2019) and the sequential conversion of IO⁻ to more oxidized forms as described by equation R8-R10.

225   Having established that all of the expected $IO_X^-$ anions are present in our IMR, we can propose a route for $HNO_3$ detection as $NO_3^-$ which involves transfer of a proton from $HNO_3$ (a very strong acid) to the conjugate base of the respective iodine containing acids (hypoiodous-, iodous- and iodic-acid):

$$IO^- + HNO_3 \quad \rightarrow \quad NO_3^- + HOI \quad\quad\quad\quad\quad\quad\quad\quad\quad\quad\quad\quad\quad (R14)$$

$$IO_2^- + HNO_3 \quad \rightarrow \quad NO_3^- + HOIO \quad\quad\quad\quad\quad\quad\quad\quad\quad\quad\quad\quad (R15)$$

230   $$IO_3^- + HNO_3 \quad \rightarrow \quad NO_3^- + HOIO_2 \quad\quad\quad\quad\quad\quad\quad\quad\quad\quad\quad (R16)$$

Taking $IO_3^-$ as an example, we see that the net reaction, ($I^- + O_3 + HNO_3 \rightarrow NO_3^- + HOIO_2$) is driven by the relative stability of iodic acid compared to $O_3$, thus bypassing the thermodynamic barrier to direct formation of $NO_3^-$ from $HNO_3 + I^-$. Using heats of formation (in kJ mol⁻¹ at 298 K) of $\Delta H_f(IO_3^-)$ = -211 (Eger et al., 2019), $\Delta H_f(HNO_3)$ = -134 (Goos et al., 2005), $\Delta H_f(HOIO_2)$ = -95 (Khanniche et al., 2016) and $\Delta H_f(NO_3^-)$ = -312 (Goos et al., 2005) we calculate that reaction R16

235   is exothermic by ~62 kJ mol⁻¹.

As described above, the $O_3$ dependence of the ion signals we observe for $IO^-$, $IO_2^-$ and $IO_3^-$ are consistent with the sequential oxidation of $I^-$ by $O_3$. However, the relative ion-abundance we observe at the detector does not necessarily reflect the relative concentration of the ions in the IMR and we cannot assign the individual contribution of any single $IO_X^-$ anion to $HNO_3$ detection. We are unable to completely shut of collisional dissociation in our I-CIMS which may be a characteristic that is

240   peculiar to our instrument as we do not detect weakly-bound $I^-(R(O)OH)$ clusters which are commonly monitored in other instruments utilising $I^-$ chemical ionisation (Lee et al., 2014). Hence, our relative sensitivity to the $IO_X^-$ components is unknown.

In order to confirm that $IO_X^-$ is responsible for detection of $HNO_3$ we examined the depletion of the signals at *m/z* 143, *m/z* 159 and *m/z* 175 when adding very large concentrations of $HNO_3$ to the IMR. The results, summarised in Fig. 5, indicate that

245   all three $IO_X^-$ ions are removed when the $HNO_3$ mixing ratio was increased from zero to 80 ppbv, but with different fractional changes. This can be understood if e.g. the individual $IO_X^-$ react with $HNO_3$ with different rate coefficients. The solid lines in Fig. 5 represent exponential decays of each ion, with rate coefficients of ~10 × 10⁻¹⁰ cm³ molecule⁻¹ s⁻¹ for $HNO_3 + IO_3^-$, ~7 × 10⁻¹⁰ cm³ molecule⁻¹ s⁻¹ for $HNO_3 + IO_2^-$ and ~3 × 10⁻¹⁰ cm³ molecule⁻¹ s⁻¹ for $HNO_3 + IO^-$. These approximate values were derived by converting the $HNO_3$ mixing ratio into a concentration in the IMR and assuming

250   pseudo-first-order behaviour (i.e. negligible depletion of $HNO_3$) so that (using $IO_3^-$ as example):

$$S(IO_3^-)_t = S(IO_3^-)_0 \exp(-kt[HNO_3]_{IMR})$$

Where $S(IO_3^-)_t$ and $S(IO_3^-)_0$ are the signals at *m/z* 175 after and prior to addition of $HNO_3$, respectively. $[HNO_3]_{IMR}$ is the concentration (molecule cm⁻³) of $HNO_3$ in the IMR, *k* (cm³ molecule⁻¹ s⁻¹) is the rate coefficient for reaction between $HNO_3$ and $IO_3^-$ and *t* is the reaction time, which we assume to be 25 ms (see above). This analysis assumes that the re-establishment

255   of equilibria between $IO_X^-$ is minimal on the time scale of the reaction between any single $IO_X^-$ and $HNO_3$. The results

indicate qualitatively that $IO_3^-$ is the most reactive of the $IO_X^-$ anions towards $HNO_3$, but that all three contribute to $HNO_3$ detection. The depletion of the summed $IO_X^-$ signals versus the accompanying increase in signal due to $NO_3^-$ at $m/z$ 62 is displayed in Fig. 6, which indicates a roughly linear relationship, confirming that $IO_X^-$ are mainly responsible for detection of $HNO_3$ in our I-CIMS. We note that the absolute increase in signal at $m/z$ 62 is about a factor of 100 greater than the reduction in the signal from $IO_X^-$, implying that the detection of $IO_3^-$ in our instrument is inefficient.

While the reactions of $IO_X^-$ with $HNO_3$ represent the most likely route to $HNO_3$ detection at $m/z$ 62 in our CIMS other possibilities are the reactions of oxide, superoxide and ozone anions ($O_X^-$) and hydrated $O_X^-$ with $HNO_3$ as they have large rate coefficients ($> 10^{-9}$ cm$^3$ molecule$^{-1}$ s$^{-1}$) and form $NO_3^-$ (Huey, 1996; Wincel et al., 1996; Lengyel et al., 2020):

$$O^- + HNO_3 \quad \rightarrow \quad NO_3^- + OH \qquad\qquad\qquad\qquad (R17)$$

$$O_2^- + HNO_3 \quad \rightarrow \quad NO_3^- + HO_2 \qquad\qquad\qquad\qquad (R18)$$

$$O_3^- + HNO_3 \quad \rightarrow \quad NO_3^- + \text{neutrals} \qquad\qquad\qquad\qquad (R19)$$

However, when adding $O_3$ (up to 600 ppbv) to the IMR we saw no signal that could be attributable to any oxide anion $O_X^-$.

Figure 7a displays the dependence of the $NO_3^-$ signal at $m/z$ 62 on the $O_3$ mixing ratio with $HNO_3$ held constant at 40 ($\pm$ 6) ppbv. The dependence of the normalised signal at $m/z$ 62 on $[O_3]$ is clearly non-linear. We showed above that the sum of all $IO_X^-$ anions increases approximately linearly with $O_3$ mixing ratio while at the same time the behaviour of $IO^-$ and $IO_3^-$ is more complex. The sensitivity of $HNO_3$ detection to changes in $O_3$ concentration is expected to depend not only on the individual concentrations of each anion in the IMR but also on their respective rate coefficients for reaction with $HNO_3$ (which are different, see above) and the observed non-linearity is not surprising. The solid lines through the data points are regressions of the form:

$$\text{Signal } (m/z\ 62) = A(1-\exp(-[O_3]B)) \qquad\qquad\qquad\qquad (2)$$

Which reflects the expected, approximately exponential dependence of the concentration of $IO_x^-$ in the IMR on the $O_3$ concentration. In equation 2, $[O_3]$ is the $O_3$ mixing ratio in ppbv and $B$ has a value of $1.515 \times 10^{-3}$ per ppbv of $O_3$. As shown in Fig 7b, for a given $[HNO_3]$, the parameter $A$ is dependent on the water vapour concentration (i.e. on ratio of signals at $m/z$ 145 and $m/z$ 127, ($S_{145}$ / $S_{127}$) over the range explored and can be parameterised as:

$$A = 0.138 + 0.929 \times (S_{145} / S_{127}) \qquad\qquad\qquad\qquad (3)$$

In these experiments, $H_2O$ was not added to the TD inlet (this would have increased the retention time of $HNO_3$ on inlet surfaces, thereby making changes in the $m/z$ 62 difficult to interpret) but directly to the IMR, as described in section 2 and as used during airborne operation of the CIMS. The linear dependence of the signal at $m/z$ 62 on the ratio of signals at $m/z$ 145 and $m/z$ 127 at various ozone concentrations ($[HNO_3]$ fixed at 38.5 ppbv) is further highlighted in Fig S3.

The positive intercept in Fig. 7b indicates that there is significant sensitivity to $HNO_3$ detection at $m/z$ 62 in the absence of water in the IMR, implying that $IO_X^-$ anions can react directly with $HNO_3$ to form $NO_3^-$ as written in R14-16. The increase in the sensitivity to $HNO_3$ as the water vapour concentration is increased is consistent with the formation of $I^-(H_2O)$ ($m/z$ 145)

which reacts more rapidly with $O_3$ (to form $IO_2^-$ directly) than does $I^-$ (Teiwes et al., 2019), thereby increasing the abundance of $IO_X^-$ in the IMR (see above) and thus the instrument's sensitivity to $HNO_3$.

290    The very strong sensitizing effect of ozone and $H_2O$ vapour can explain why similar instruments to ours observe large signals at *m/z* 62 when sampling ambient air. Indeed, both $O_3$ and $HNO_3$ are ubiquitous and generally present at much higher levels than either $NO_3$ or $N_2O_5$. Attempts to measure these traces gases using I-CIMS without TD-inlets and NO titration (to remove the $HNO_3$ contribution) will likely result in erroneously high levels of both, especially during the day when lower-tropospheric $O_3$ and $HNO_3$ are often at their highest levels. It also explains why laboratory tests (generally carried out

295    without added $O_3$ or $H_2O$) have shown only low (or no) sensitivity to $HNO_3$ at *m/z* 62.

## 3.2 Detection of HNO₃ at *m/z* 190

We now compare the detection of $HNO_3$ at *m/z* 62 to its detection at *m/z* 190, the $I^-(HNO_3)$ adduct, with various amounts of $O_3$ present. In Fig. 8 we present the results of an experiment in which a constant flow of $HNO_3$ (12.5 ppbv) was introduced into the inlet and the ozone mixing ratio was varied from zero to 900 ppbv. We observe a great increase in the signal at *m/z*

300    62 as expected (from 9 counts to > 6000 counts). At zero ozone, the signal at *m/z* 190 is about 1000 counts and is largely background free, making this the preferred mass to monitor $HNO_3$ in the absence of $O_3$. The cross-over point (when the signals at *m/z* 62 and *m/z* 190 are equal) is at an ozone mixing ratio of 100 ppbv. At an ozone mixing ratio of 800 ppbv, the signal at *m/z* 62 is a factor 8.5 larger than that at *m/z* 190.

Apparent from this figure is the depletion of the signal at *m/z* 190 as the $O_3$ mixing ratio increases to values of 800 ppbv, as

305    present e.g. in the lower stratosphere. The solid lines are least-squares fits to the datasets that describe the exponential growth of the *m/z* 62 signal as $O_3$ is increased and the exponential decay of *m/z* 190 over the same range. The reduction in signal at *m/z* 190 is characterised by an exponential term $\exp(-0.00046 \times [O_3])$ which means that at 800 ppbv $O_3$ a ~30% reduction in sensitivity is observed. The loss of sensitivity at *m/z* 190 is driven by the loss of $I^-$ in the IMR as $O_3$ is added. At the same time, the depletion of the signal at *m/z* 127 is weaker, which reflects the fact that only a small fraction of $IO_X^-$

310    formed in the IMR are detected, the rest presumably being fragmented in the CDC before being detected as $I^-$.

The fact that some $I^-$ is converted to $IO_X$ in the IMR at high $O_3$ levels but is not reflected in the $I^-$ signal at *m/z* 127 has repercussions for normalisation of product ion signals to the primary ion signal whereby the assumption is made that the measured signal at *m/z* 127 stems only from $I^-$. In our instrument, the loss of $I^-$ in the IMR is significant at high levels of $O_3$ (e.g. 30 % at 800 ppbv $O_3$). For this reason, we normalise the signals using values of the signal at *m/z* 127 obtained by

315    interpolating between measurements obtained when scrubbing the air. The normalisation problem may occur in other I-CIMS instruments to varying extents, and the degree of bias will depend on the conversion of $I^-$ to $IO_X^-$ and the extent to which $IO_X^-$ is detected as $I^-$. The potential bias can be circumvented by the continuous addition of a calibration gas that is detected via reaction with $I^-$.

**3.3 Detection of HNO₃ at *m/z* 62: The role of acetate anions**

320   We have also evaluated the potential for "unintentional" $HNO_3$ detection at *m/z* 62 by its reaction with the acetate anion, $CH_3CO_2^-$:

$$CH_3CO_2^- + HNO_3 \qquad \rightarrow \qquad NO_3^- + CH_3C(O)OH \tag{R20}$$

The $CH_3CO_2^-$ anion is the conjugate base of a weak acid ($CH_3C(O)OH$) has been utilised to monitor a number of trace gases via proton transfer (Veres et al., 2008). While Veres et al. (2010) generated $CH_3CO_2^-$ deliberately by passing acetic-

325   anhydride through their $^{210}$Po-source, in our experiments it is the product (monitored at *m/z* 59) of the reaction between I⁻ primary ions and either $CH_3C(O)O_2$ (from the thermal dissociation of PAN) or $CH_3C(O)OOH$.

$$I^- + CH_3C(O)O_2 \qquad \rightarrow \qquad CH_3CO_2^- + IO \tag{R21}$$

$$I^- + CH_3C(O)OOH \qquad \rightarrow \qquad CH_3CO_2^- + HOI \tag{R22}$$

Figure 9a shows the result of a set of experiments demonstrating $HNO_3$ detection at *m/z* 62 without (blue data points) and

330   with 3.25 ppbv of $CH_3C(O)OOH$ (black data points) added to the inlet flow. The initial (normalised) signal at *m/z* 59 from the $CH_3CO_2^-$ anion in the absence of $HNO_3$ was 53500 counts. The presence of 3.25 ppbv $CH_3C(O)OOH$ (and resultant $CH_3CO_2^-$) results in a ~50-fold increase in the sensitivity of the I-CIMS to $HNO_3$. We also carried out a few experiments (less systematic) in which PAN (instead of PAA) was added to the IMR and obtained the same results.

Our results disagree with the conclusions of Wang et al. (2014) who saw no increase at *m/z* 62 when adding PAN to air

335   containing $HNO_3$ but are consistent with the use of $CH_3CO_2^-$ as primary reactant ion to detect $HNO_3$ at *m/z* 62 (Veres et al., 2008). Figure 9b indicates that the increase in signal at *m/z* 62 when adding $HNO_3$ to a flow of $CH_3C(O)OOH$ in air is approximately proportional to the reduction in the ion-signal at *m/z* 59. This helps confirm that $CH_3CO_2^-$ is the ion responsible for the detection of $HNO_3$ but also indicates that the detection of PAN and $CH_3C(O)OOH$ via conversion to $CH_3CO_2^-$ can be compromised when $HNO_3$ is present in the air sample. Indeed, in many air masses the concentration of

340   $HNO_3$ can be an order of magnitude greater than that of either PAN or $CH_3C(O)OOH$ and given that other abundant trace gases (e.g. organic acids) also react with $CH_3CO_2^-$ (Veres et al., 2008) further reactions of $CH_3CO_2^-$ in the ion-molecule reactor regions of I-CIMS instruments may result in a significant bias (to lower values) which would have to be analysed case-by-case for different instruments. One way to avoid this problem is the continuous addition of isotopically labelled PAN to the inlet  (see e.g. Roiger et al. (2011)) as the secondary, reactive losses of  $^{12}$C and $^{13}$C $CH_3CO_2^-$ are expected to be

345   identical.

Wang et al. (2014) observed that the majority of the *m/z* 62 signal during the daytime could be removed by addition of NO (0.54 ppmv or $1.3 \times 10^{13}$ molecule $cm^{-3}$) to the inlet. At their inlet temperature of 120-180 °C, NO reacts with $O_3$ with a rate coefficient in the range $6\text{-}9 \times 10^{-14}$ $cm^3$ molecule$^{-1}$ s$^{-1}$, which results in a half-life for $O_3$ of 500 to 800 ms. Wang et al. (2014) do not mention the residence time of air passing through their heated inlet, but it appears plausible that a substantial fraction

350   of ambient $O_3$ would have been removed during background measurement, thus decreasing (or removing) sensitivity towards

$HNO_3$ via reactions involving $O_3$ in the IMR, and leading the authors to conclude that $NO_3$ was being detected above a lower background than truly present.

To illustrate the potential size of the bias due to $HNO_3$ when monitoring $N_2O_5$ at $m/z$ 62 in field measurements we take the relative sensitivities (at $m/z$ 62) of our I-CIMS to $N_2O_5$ and to $HNO_3$ (in the presence of typical boundary layer mixing ratios of $O_3$ (50 ppbv) and at typical relative humidity (50%). Under these conditions, with $N_2O_5$ and $HNO_3$ mixing ratios of 0.2 and 2 ppbv, respectively, we calculate that $HNO_3$ would account for > 70% of the signal at $m/z$ 62.

## 4 Field Measurements

Having shown that $HNO_3$ is detected by our I-CIMS with reasonable sensitivity when sufficient $O_3$ is present in ambient air samples, we now examine the signals at $m/z$ 62 obtained in airborne operation of the I-CIMS during two CAFE (Chemistry of the Atmosphere Field Experiment) campaigns of the HALO aircraft. In the CAFE-Africa campaign (2018) the I-CIMS monitored $m/z$ 62 on several flights over the Atlantic west of the African continent. During the 2020 CAFE-EU campaign with HALO over Europe, the I-CIMS additionally monitored $m/z$ 190 (the $I^-(HNO_3)$ cluster ion) which is selective to $HNO_3$. During both campaigns, $O_3$ and $H_2O$ (required for analysis of the signal at $m/z$ 62) were routinely measured.

### 4.1 CAFÉ-Africa

Here we examine the results obtained during a HALO flight as part of the CAFE-Africa mission. The flight in question was the transfer from Sal airport on the Cape Verde islands (which served as base-station during the mission) back to Germany. During the flight the aircraft flew mainly at high altitudes (13-15 km) so that stratospheric air was sampled at higher latitudes but also made two dives into the free-troposphere. The flight track is displayed in Fig S4.

Figure 10 shows a time-series of ozone mixing ratios during the flight (panel a) along with the I-CIMS signal at $m/z$ 62 (panel b). In air masses with stratospheric influence (i.e. $O_3$ values > 100 ppb, 12:20 -15:10 UTC) there is an obvious, strong co-variance between these two parameters. However, once corrected for the dependence of the sensitivity of the I-CIMS to $O_3$ (equations 2 and 3) we obtain the black line representing the mixing ratios of $HNO_3$ and the covariance is greatly reduced. We also note that, apart from some significant increases at ~11:30 and ~16:00 the $HNO_3$ mixing ratio decreases slowly throughout the flight, which is the result of $HNO_3$ generation in the [210]Po source leading to an initially large background signal. The formation of $HNO_3$ in the [210]Po source has been documented previously (Ji et al., 2020); its level can be reduced by permanently flushing $N_2$ through the source while keeping the mass-spectrometer under operational vacuum. This was not carried out during the CAFE missions on HALO as continuous operation of the instrument (i.e. overnight between flights) was not possible. We note that the background signal at $m/z$ 62 that originates from the polonium source cannot be obtained by scrubbing the air of $HNO_3$ as this also removes $O_3$ and thus also sensitivity to $HNO_3$ at this mass.

380     A roughly exponential decay of the $HNO_3$ background signal was observed in all of the flights in which $m/z$ 62 was monitored, which presumably reflects depletion of the initially large $HNO_3$ reservoir which was built up when the I-CIMS was switched off.

    A coarse correction of the dataset was thus undertaken by subtracting an exponentially decaying background from the total $HNO_3$ signal. The resulting $HNO_3$ mixing ratios are depicted as the blue line in Fig. 10b and plotted against the $O_3$ mixing

385  ratio in Fig. 10c. Considering only the high altitude data for which $O_3$ mixing ratios were > 100 ppbv (stratospheric influence, black data points) we derive a slope of $HNO_3 / O_3 = (3 \pm 0.5) \times 10^{-3}$ (the uncertainty is 2 $\sigma$, statistical only) which is consistent with previously reported values obtained in airborne measurements of $HNO_3$ and $O_3$ in the lower stratosphere (see Popp et al. (2009) and references therein). We stress that deriving accurate mixing ratios of $HNO_3$ is not possible with this data set and the values obtained are strongly dependent on the background correction. Here, we merely wish to indicate

390  that, while most of the variability in our $m/z$ 62 signal is related to the central role of ozone in the detection scheme (i.e. formation of $IO_X^-$), some covariance between $HNO_3$ and $O_3$ remains after correction of the raw data and the slope is roughly in line with that expected. We also do not propose that the correlation of $m/z$ 62 with $O_3$ proves that the signal can be attributed entirely to $HNO_3$. This aspect will be covered in section 4.2.

    Figure 10b reveals sharp increases in the (background corrected) $HNO_3$ mixing ratio when sampling at lower altitudes,

395  noticeably at 11:30- 12:00 (3.9 km altitude) and at 15:45-16:10 (4.7 km altitude) and at the end of the flight during descent to Oberpfaffenhofen in Bavaria, Germany. In all cases, these periods of enhanced $HNO_3$ coincided with higher levels of particles. Back trajectories (HYSPLIT) indicated that, in the 10 days prior to interception by HALO, the air mass sampled at 11:30 had passed over the West African continent (Mauritania, Mali and Niger), whereas the air masses sampled after 16:00 were of European origin. The large, coincidental increase in the $HNO_3$ mixing ratio and particle mass was a recurrent feature

400  of the CAFE-Africa flights. It is conceivable that the $HNO_3$ measured by the I-CIMS was a mixture of gas-phase $HNO_3$ and $HNO_3$ associated with particles that desorb $HNO_3$ when passing through the thermal dissociation inlet at 180 °C. This temperature would be sufficient to thermally convert ammonium nitrate to $HNO_3$ (and $NH_3$) as well as to result in the desorption of $HNO_3$ that was physi-sorbed e.g. on chemically aged black-carbon or mineral-dust particles. As we do not know the efficiency with which particles of various diameters enter the TD-inlet of the CIMS, we cannot estimate the

405  relative contribution of gas-phase and particulate nitrate to the signal at $m/z$ 62 but indicate that a similar phenomenon may occur in ground-based measurements using TD-inlets and may represent an additional source of bias during ambient measurements of $NO_3$ and/or $N_2O_5$ at $m/z$ 62.

## 4.2 CAFE-Europa

    During the CAFE-Europe HALO flights the I-CIMS monitored $m/z$ 190, the $I^-(HNO_3)$ adduct, as well as $NO_3^-$ at $m/z$ 62. The

410  detection of $HNO_3$ at $m/z$ 190 varies with the water vapour concentration in the IMR: The response of the $HNO_3$ signal at $m/z$ 190 to changes in the $HNO_3$ concentration and in the $m/z$ 145 / $m/z$ 127 ratio (i.e. the relative humidity in the IMR, see Fig. S2) is illustrated in Fig. S5.

Figure 11 displays a set of data obtained during a flight on the 30th May 2020 on which the HALO aircraft flew a path from Southern Germany to the Atlantic (west of Ireland) and back at various altitudes (for flight track see Fig S6). Figure 11a plots the raw signals measured by the I-CIMS at $m/z$ 62 and $m/z$ 190 as well as the $O_3$ mixing ratio. Similar to the CAFE-Africa dataset, the signal at $m/z$ 62 covaries strongly with the $O_3$ mixing ratios, which were between ~40 and ~700 ppbv whereas the raw signals at $m/z$ 62 and $m/z$ 190 (both due to $HNO_3$) bear little resemblance to each other.

Using the calibration parameters described in section 3 and (for $m/z$ 190) in Fig. S3, the signals at $m/z$ 62 and $m/z$ 190 were converted to $HNO_3$ mixing ratios, depicted in Fig. 11b. Despite the greatly divergent raw-signals, the $HNO_3$ mixing ratios obtained using the different mass-to-charge ratios are in reasonable agreement, both displaying a gradual decrease after take-off at ~08:00 UTC. The high initial level of $HNO_3$ is largely the result of $HNO_3$ being formed in the $^{210}Po$ source during overnight instrument shut-down (see section 4.1). The $HNO_3$ mixing ratios observed at $m/z$ 62 and $m/z$ 190 both increase when the aircraft sampled stratospheric air (11:00 to 13:00 and 15:10-15:30 UTC). In Fig. 11c $HNO_3$ mixing ratios derived at $m/z$ 62 and $m/z$ 190 are plotted in a correlation diagram. The slope (1.14 ± 0.05) and intercept (-0.3 ± 0.3) indicate reasonable agreement even when the raw signals are greatly divergent at high levels of $O_3$. At the highest levels of $O_3$, some differences in the retrieved mixing ratios of $HNO_3$ using $m/z$ 62 and $m/z$ 190 are observed, which, given the large, $O_3$-dependent corrections applied (especially for $m/z$ 62) is not surprising. Our airborne data show that in many (if not most) air masses, $m/z$ 62 provides a measure of $HNO_3$ rather than $NO_3$ and $N_2O_5$.

## 5 Conclusions

A series of laboratory experiments investigating the origin of signal at $m/z$ 62 when using an I-CIMS has revealed unexpected sensitivity to $HNO_3$ at this mass-to-charge ratio in the presence of $O_3$ or peroxyacetic acid (PAA) or PAN. The ozone effect is related to the formation of $IO_X^-$ which react rapidly with $HNO_3$ to form $NO_3^-$ thus bypassing the thermodynamic barrier to formation of $NO_3^-$ by direct reaction of $HNO_3$ with $I^-$. The presence of $O_3$ at a mixing ratio of 500 ppbv results in a 250-fold increase in sensitivity to $HNO_3$ at $m/z$ 62. The sensitivity to $HNO_3$ at this mass-to-charge ratio was also found to be highly dependent on the concentration of $H_2O$ in the ion-molecule reactor as this aids formation of $IO_X^-$. The sensitivity to $HNO_3$ at $m/z$ 62 in the presence of PAA is a result of the presence of acetate anions ($CH_3CO_2^-$) as demonstrated previously (Veres et al., 2008). We conclude that measurements of PAN using I-CIMS may be biased to low values if large mixing ratios of $HNO_3$ (or organic acids) are present and continuous calibration (e.g. with isotopically labelled PAN) is not carried out. Our laboratory experiments indicate that measurements of atmospheric $NO_3$ and $N_2O_5$ at $m/z$ 62 can be heavily biased by the presence of $HNO_3$, and may explain reports of unexpectedly high daytime mixing ratios of $N_2O_5$. The relative sensitivity at $m/z$ 62 to $HNO_3$ and $N_2O_5$ / $NO_3$ will vary from one I-CIMS instrument to the next and must thus be analysed case-by-case.

We have examined signals at $m/z$ 62 during two periods of operation of the I-CIMS on the HALO-aircraft, one over the Atlantic west of the African coast and one over Europe. During the flights over Europe $HNO_3$ mixing ratios derived from $m/z$

445  62  $NO_3^-$  and at $m/z$ 190 ($I^-(HNO_3)$)) were in good agreement. The data obtained over the Atlantic indicated that measurements at $m/z$ 62 using a thermal dissociation inlet can be strongly influenced by particulate nitrate that can thermally dissociate (or desorb) to gas-phase $HNO_3$.

## Data availability

Data measured during the flight campaign CAFE campaigns are available to all scientists agreeing to the CAFE data
450  protocol. The laboratory data underlying the Figures is available upon request to the authors.

## Author contributions

RD conducted the laboratory experiments, carried out the airborne measurements with assistance from PE and JC and analysed the laboratory data with assistance from JC. The manuscript was written by JC and RD with contributions from all other authors. JL designed and helped plan the airborne operations.

455  ## Competing interests

The authors declare that they have no conflict of interest.

## Acknowledgments

460  We acknowledge the collaboration with the DLR (German Aerospace Centre) during the HALO campaigns CAFE- Africa and CAFE-EU. We thank Florian Obersteiner and Andreas Zahn (KIT-Karlsruhe) for use of the $O_3$-data during CAFE-Africa and CAFE-EU.

## References

Atkinson, R., Baulch, D. L., Cox, R. A., Crowley, J. N., Hampson, R. F., Hynes, R. G., Jenkin, M. E., Rossi, M. J., and Troe,
465  J.: Evaluated kinetic and photochemical data for atmospheric chemistry: Volume I - gas phase reactions of O$x$, HO$x$, NO$x$ and SO$x$ species, Atmos. Chem. Phys., 4, 1461-1738, doi:10.5194/acp-4-1461-2004, 2004.

Bhujel, M., Marshall, D. L., Maccarone, A. T., McKinnon, B. I., Trevitt, A. J., da Silva, G., Blansby, S. J., and Poad, B. L. J.: Gas phase reactions of iodide and bromide anions with ozone: evidence for stepwise and reversible reactions, Phys. Chem. Chem. Phys., 22, 9982-9989, doi:10.1039/d0cp01498b, 2020.

470  Chang, W. L., Bhave, P. V., Brown, S. S., Riemer, N., Stutz, J., and Dabdub, D.: Heterogeneous atmosperic chemistry, ambient measurements and model calculatuons of $N_2O_5$: A review, Aerosol. Sci. Tech, 45, 655-685, doi:10.1080/02786826.2010.551672, 2011.

Crowley, J. N., Ammann, M., Cox, R. A., Hynes, R. G., Jenkin, M. E., Mellouki, A. M., Rossi, M. J., Troe, J., and Wallington, T. J.: Evaluated kinetic and photochemical data for atmospheric chemistry: Volume V - heterogeneous reactions
475  on solid substrates, Atmos. Chem. Phys., 10, 9059-9223, 2010.

Davidson, J. A., Viggiano, A. A., Howard, C. J., Dotan, I., Fehsenfeld, F. C., Albritton, D. L., and Ferguson, E. E.: Rate Constants for Reactions of $O_2^+$, $NO_2^+$, $NO^+$, $H_3O^+$, $CO_3^-$, $NO_2^-$, and Halide Ions with $N_2O_5$ at 300 K, J. Chem. Phys., 68, 2085-2087, 1978.

480 Dubé, W. P., Brown, S. S., Osthoff, H. D., Nunley, M. R., Ciciora, S. J., Paris, M. W., McLaughlin, R. J., and Ravishankara, A. R.: Aircraft instrument for simultaneous, in situ measurement of $NO_3$ and $N_2O_5$ via pulsed cavity ring-down spectroscopy, Rev. Sci. Instrum., 77, doi: 10.1063/1.2176058, 2006.

Dulitz, K., Amedro, D., Dillon, T. J., Pozzer, A., and Crowley, J. N.: Temperature-(208-318 K) and pressure-(18-696 Torr) dependent rate coefficients for the reaction between OH and $HNO_3$, Atmos. Chem. Phys., 18, 2381-2394, 2018.

Eger, P. G., Helleis, F., Schuster, G., Phillips, G. J., Lelieveld, J., and Crowley, J. N.: Chemical ionization quadrupole mass 485 spectrometer with an electrical discharge ion source for atmospheric trace gas measurement, Atmos. Meas. Tech., 12, 1935-1954, doi:10.5194/amt-12-1935-2019, 2019.

Fehsenfeld, F. C., Howard, C. J., and Schmeltekopf, A. L.: Gas phase ion chemistry of $HNO_3$, The Journal of Chemical Physics, 63, 2835-2841, doi:10.1063/1.431722, 1975.

Fischer, H., Waibel, A. E., Welling, M., Wienhold, F. G., Zenker, T., Crutzen, P. J., Arnold, F., Burger, V., Schneider, J., 490 Bregman, A., Lelieveld, J., and Siegmund, P. C.: Observations of high concentrations of total reactive nitrogen (NOy) and nitric acid ($HNO_3$) in the lower Arctic stratosphere during the stratosphere-troposphere experiment by aircraft measurements (STREAM) II campaign in February 1995, J. Geophys. Res. -Atmos., 102, 23559-23571, doi:10.1029/97jd02012, 1997.

Goos, E., Burcat, A., and Ruscic, B.: Extended Third Millennium Ideal Gas and Condensed Phase Thermochemical Database for Combustion with Updates from Active Thermochemical Tables: Update of "Third Millennium Ideal Gas and Condensed 495 Phase Thermochemical Database for Combustion with Updates from Active Thermochemical Tables by Alexander Burcat and Branko Ruscic", Report ANL 05/20 and TAE 960 Technion-IIT, Aerospace Engineering, and Argonne National Laboratory, Chemistry Division, September 2005., 2005.

Hanson, D. R., and Ravishankara, A. R.: The reaction probabilities of $ClONO_2$ and $N_2O_5$ on polar stratospheric cloud material, JGR, 96, 5081-5090, 1991.

500 Huey, L. G., Hanson, D. R., and Howard, C. J.: Reactions of $SF_6^-$ and $I^-$ with atmospheric trace gases, J. Phys. Chem., 99, 5001-5008, doi:10.1021/j100014a021, 1995.

Huey, L. G.: The kinetics of the reactions of $Cl^-$, $O^-$, and $O_2^-$ with $HNO_3$: Implications for measurement of $HNO_3$ in the atmosphere, Int. J. Mass Spectrom. Ion Processes, 153, 145-150, doi:10.1016/0168-1176(95)04354-3, 1996.

Huey, L. G.: Measurement of trace atmospheric species by chemical ionization mass spectrometry: Speciation of reactive 505 nitrogen and future directions, Mass Spectrom. Rev., 26, 166-184, doi:10.1002/mas.20118, 2007.

Task Group on Atmospheric Chemical Kinetic Data Evaluation, (Ammann, M., Cox, R.A., Crowley, J.N., Herrmann, H., Jenkin, M.E., McNeill, V.F., Mellouki, A., Rossi, M. J., Troe, J. and Wallington, T. J.): http://iupac.pole-ether.fr/index.html., 2021.

Iyer, S., He, X. C., Hyttinen, N., Kurten, T., and Rissanen, M. P.: Computational and experimental investigation of the 510 detection of $HO_2$ radical and the products of its reaction with cyclohexene ozonolysis derived $RO_2$ radicals by an iodide-based chemical ionization mass spectrometer, J. Phys. Chem. A, 121, 6778-6789, doi:10.1021/acs.jpca.7b01588, 2017.

Ji, Y., Huey, L. G., Tanner, D. J., Lee, Y. R., Veres, P. R., Neuman, J. A., Wang, Y., and Wang, X.: A vacuum ultraviolet ion source (VUV-IS) for iodide–chemical ionization mass spectrometry: a substitute for radioactive ion sources, Atmos. Meas. Tech., 13, 3683-3696, doi:10.5194/amt-13-3683-2020, 2020.

515 Kercher, J. P., Riedel, T. P., and Thornton, J. A.: Chlorine activation by $N_2O_5$: simultaneous, in situ detection of $ClNO_2$ and $N_2O_5$ by chemical ionization mass spectrometry, Atmos. Meas. Tech., 2, 193-204, doi:10.5194/amt-2-193-2009, 2009.

Khanniche, S., Louis, F., Cantrel, L., and Černušák, I.: A theoretical study of the microhydration of iodic acid (HOIO2), Computational and Theoretical Chemistry, 1094, 98-107, doi:https://doi.org/10.1016/j.comptc.2016.09.010, 2016.

Lee, B. H., Lopez-Hilfiker, F. D., Mohr, C., Kurten, T., Worsnop, D. R., and Thornton, J. A.: An iodide-adduct high-resolution time-of-flight chemical-ionization mass spectrometer: Application to atmospheric inorganic and organic compounds, Env. Sci. Tech., 48, 6309-6317, doi:10.1021/es500362a, 2014.

Lengyel, J., Oncak, M., and Beyer, M. K.: Chemistry of $NO_X$ and $HNO_3$ molecules with gas-phase hydrated $O^-$ and $OH^-$ ions, Chemistry-a European Journal, 26, 7861-7868, doi:10.1002/chem.202000322, 2020.

Lightfoot, P. D., Cox, R. A., Crowley, J. N., Destriau, M., Hayman, G. D., Jenkin, M. E., Moortgat, G. K., and Zabel, F.: Organic peroxy radicals - kinetics, spectroscopy and tropospheric chemistry, Atmos. Environ., Part A, 26, 1805-1961, 1992.

McCracken, F. L.: Total collision cross sections of negative atomic iodine ions in nitrogen and argon, 1952.

Phillips, G. J., Pouvesle, N., Thieser, J., Schuster, G., Axinte, R., Fischer, H., Williams, J., Lelieveld, J., and Crowley, J. N.: Peroxyacetyl nitrate (PAN) and peroxyacetic acid (PAA) measurements by iodide chemical ionisation mass spectrometry: first analysis of results in the boreal forest and implications for the measurement of PAN fluxes, Atmos. Chem. Phys., 13, 1129-1139, doi:doi:10.5194/acp-13-1129-2013, 2013.

Popp, P. J., Marcy, T. P., Gao, R. S., Watts, L. A., Fahey, D. W., Richard, E. C., Oltmans, S. J., Santee, M. L., Livesey, N. J., Froidevaux, L., Sen, B., Toon, G. C., Walker, K. A., Boone, C. D., and Bernath, P. F.: Stratospheric correlation between nitric acid and ozone, J. Geophys. Res. -Atmos., 114, 10, doi:10.1029/2008jd010875, 2009.

Riva, M., Rantala, P., Krechmer, J. E., Peräkylä, O., Zhang, Y., Heikkinen, L., Garmash, O., Yan, C., Kulmala, M., Worsnop, D., and Ehn, M.: Evaluating the performance of five different chemical ionization techniques for detecting gaseous oxygenated organic species, Atmos. Meas. Tech., 12, 2403-2421, doi:10.5194/amt-12-2403-2019, 2019.

Roiger, A., Aufmhoff, H., Stock, P., Arnold, F., and Schlager, H.: An aircraft-borne chemical ionization - ion trap mass spectrometer (CI-ITMS) for fast PAN and PPN measurements, Atmos. Meas. Tech., 4, 173-188, doi:doi:10.5194/amt-4-173-2011, 2011.

Slusher, D. L., Huey, L. G., Tanner, D. J., Flocke, F. M., and Roberts, J. M.: A thermal dissociation-chemical ionization mass spectrometry (TD-CIMS) technique for the simultaneous measurement of peroxyacyl nitrates and dinitrogen pentoxide, J. Geophys. Res. -Atmos., 109, Art Nr. D19315, doi:10.1029/2004JD004670, 2004.

Teiwes, R., Elm, J., Handrup, K., Jensen, E. P., Bilde, M., and Pedersen, H. B.: Atmospheric chemistry of iodine anions: elementary reactions of $I^-$, $IO^-$, and $IO_2^-$ with ozone studied in the gas-phase at 300 K using an ion trap, Phys. Chem. Chem. Phys., 20, 28606-28615, doi:10.1039/c8cp05721d, 2018.

Teiwes, R., Elm, J., Bilde, M., and Pedersen, H. B.: The reaction of hydrated iodide $I(H_2O)^-$ with ozone: a new route to $IO_2^-$ products, Phys. Chem. Chem. Phys., 21, 17546-17554, doi:10.1039/c9cp01734h, 2019.

Veres, P., Roberts, J. M., Warneke, C., Welsh-Bon, D., Zahniser, M., Herndon, S., Fall, R., and de Gouw, J.: Development of negative-ion proton-transfer chemical-ionization mass spectrometry (NI-PT-CIMS) for the measurement of gas-phase organic acids in the atmosphere, Int. J. Mass Spectrom., 274, 48-55, doi:10.1016/j.ijms.2008.04.032, 2008.

Veres, P., Gilman, J. B., Roberts, J. M., Kuster, W. C., Warneke, C., Burling, I. R., and de Gouw, J.: Development and validation of a portable gas phase standard generation and calibration system for volatile organic compounds, Atmos. Meas. Tech., 3, 683-691, doi:pil, 2010.

Wang, X., Wang, T., Yan, C., Tham, Y. J., Xue, L., Xu, Z., and Zha, Q.: Large daytime signals of $N_2O_5$ and $NO_3$ inferred at 62 amu in a TD-CIMS: chemical interference or a real atmospheric phenomenon?, Atmos. Meas. Tech., 7, 1-12, doi:10.5194/amt-7-1-2014, 2014.

Wayne, R. P., Barnes, I., Biggs, P., Burrows, J. P., Canosa-Mas, C. E., Hjorth, J., Le Bras, G., Moortgat, G. K., Perner, D., Poulet, G., Restelli, G., and Sidebottom, H.: The nitrate radical: Physics, chemistry, and the atmosphere, Atmos. Env. A, 25A, 1-206, 1991.

Williams, S., Campos, M. F., Midey, A. J., Arnold, S. T., Morris, R. A., and Viggiano, A. A.: Negative ion chemistry of ozone in the gas phase, J. Phys. Chem. A, 106, 997-1003, doi:10.1021/jp012929r, 2002.

Wincel, H., Mereand, E., and Castleman, A. W.: Gas phase reactions of $DNO_3$ with $X^-(D_2O)_n$, X=O, OD, $O_2$, $DO_2$, and $O_3$, J. Phys. Chem., 100, 7488-7493, doi:10.1021/jp953104i, 1996.

565
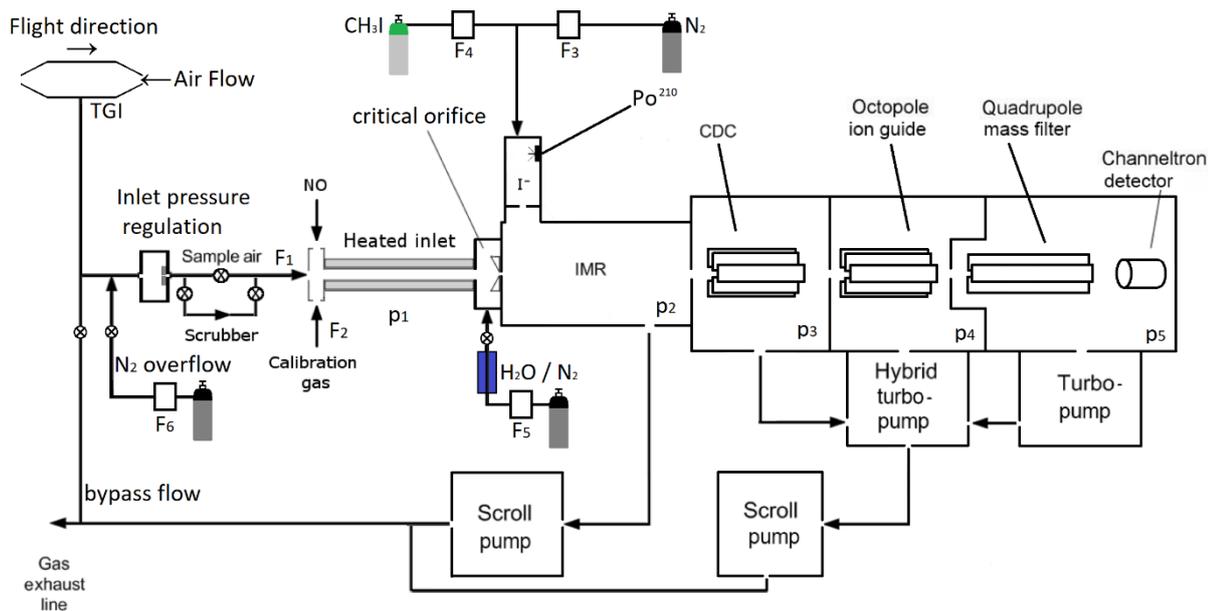
**Figure** 1 Schematic diagram illustrating the central components of the I-CIMS used in this work. IMR = ion-molecule reactor, CDC = collisional dissociation chamber, $F_1$ = 1250 cm$^3$ (STP) min$^{-1}$, $F_2$ = 50 cm$^3$ (STP) min$^{-1}$, $F_3$ = 750 cm$^3$ (STP) min$^{-1}$, $F_4$ = 4 cm$^3$ (STP) min$^{-1}$, $F_5$ = 50 cm$^3$ (STP) min$^{-1}$. p1 = 100 mbar, p2 = 24 mbar, p3 = 0.6 mbar, p4 = 6 × 10$^{-3}$ mbar, p5 = 9 × 10$^{-5}$ mbar. The heated inlet is made of PFA-tubing. TGI = Trace-gas-inlet. When overflowing the inlet line, the valve to the exhaust line is closed. When sampling air, the valve to the N$_2$ bottle is closed.

575
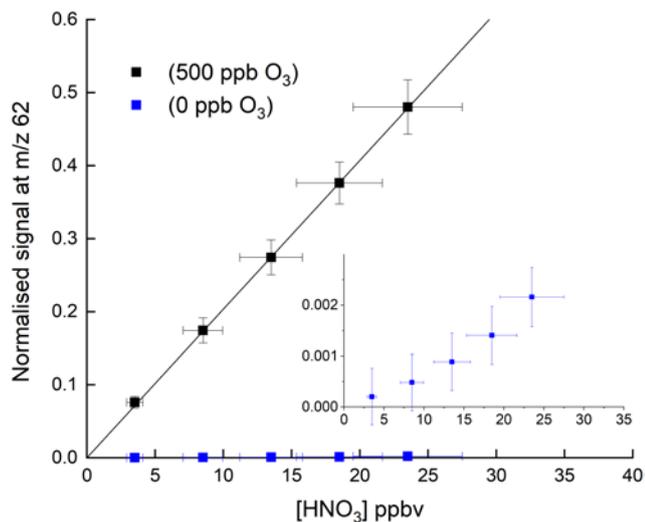
580 **Figure 2.** HNO$_3$ detection at $m/z$ 62 in the absence and presence (500 ppbv) of O$_3$. The solid lines are non-weighted, linear regressions to the data and are $2.035 \times 10^{-2}$ and $8.033 \times 10^{-5}$ ppbv$^{-1}$ HNO$_3$ when 500 ppbv O$_3$ or zero O$_3$ were present, respectively. The inset (same x- and y-axes as in the full figure) is an expanded view of the signal obtained in the absence of O$_3$. The error bars represent 15% systematic uncertainty in the HNO$_3$ concentration and $2\sigma$ statistical uncertainty in the signal at $m/z$ 62.

585
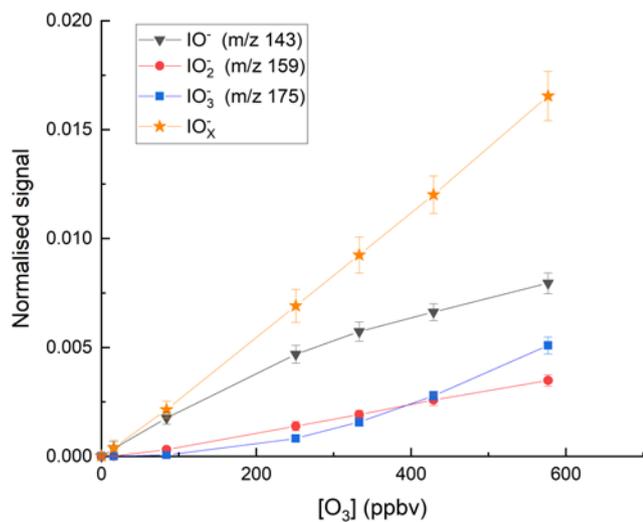
590

**Figure 3**: Variation of the I-CIMS signals at $m/z$ 143 ($IO^-$), 159 ($IO_2^-$) and 175 ($IO_3^-$) with the mixing ratios of $O_3$. The $O_3$ mixing ratios are those measured in air before the gas-flow entered the inlet. The water vapour was held constant using our standard setting ($[H_2O]_{IMR} = 2.9 \times 10^{14}$ molecule cm$^{-3}$).
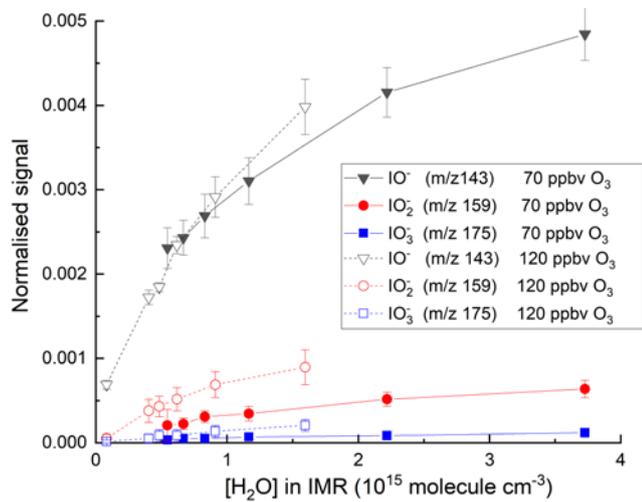
595

**Figure 4:** Variation in the total ion signal (counts) due to IO⁻, IO$_2$⁻ and IO$_3$⁻ with the concentration of water vapour in the IMR. The results are from two sets of experiments where the O$_3$ mixing ratio was either 70 or 120 ppbv.

600
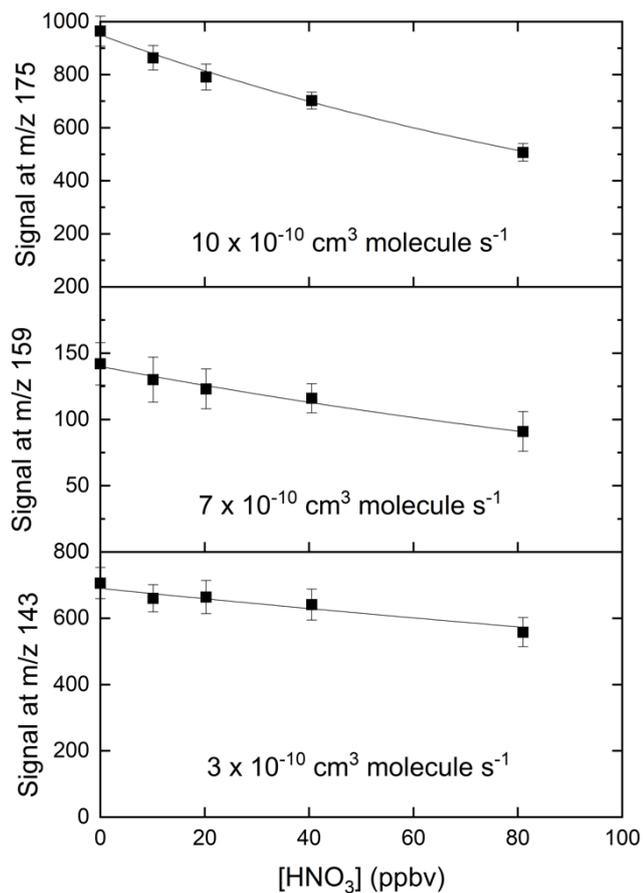
**Figure 5:** Relative changes in signals at $m/z$ 143 (IO$^-$), $m/z$ 159 (IO$_2^-$) and $m/z$ 175 (IO$_3^-$) when adding up to 80 ppbv of HNO$_3$. The rate coefficients were calculated using a reaction time of 25 ms and should thus only be regarded as approximate.

605
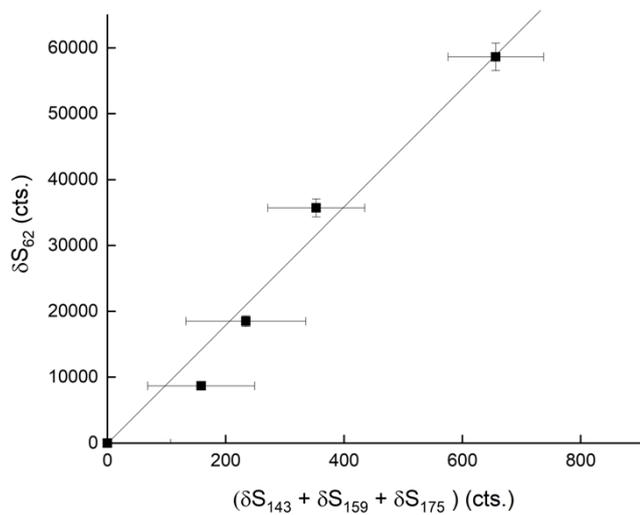
**Figure 6:** Relative changes in the sum of signals at *m/z* 143 (IO⁻), *m/z* 159 (IO₂⁻) and *m/z* 175 (IO₃⁻) when adding up to 80 ppbv of HNO₃. δ refers to the change in signal upon adding HNO₃ and thus takes background signals at each mass-to-charge ratio into account.
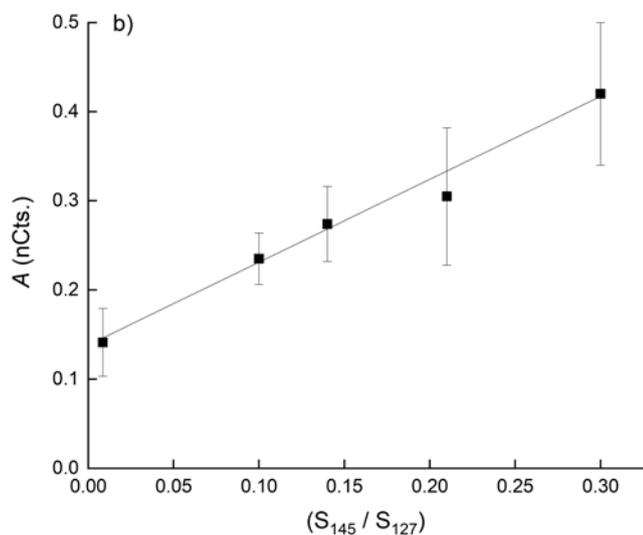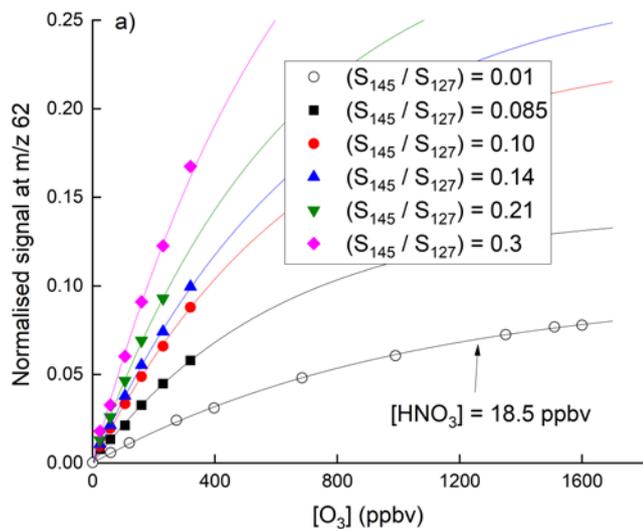
615 **Figure 7**. a) Dependence of the signal at $m/z$ 62 on the $O_3$ mixing ratio for 6 different concentrations of $H_2O$ in the IMR. In the upper 5 curves (solid symbols) the $HNO_3$ mixing ratio was 38.5 ppbv. In the lowermost curve, the $HNO_3$ mixing ratio was 18.5 ppbv, as indicated. The fits lines are of the form: $y = A*exp(1-exp(-B*[O_3]))$. b) Plot of parameter $A$ versus the relative signal at $m/z$ 145 and $m/z$ 127.

620
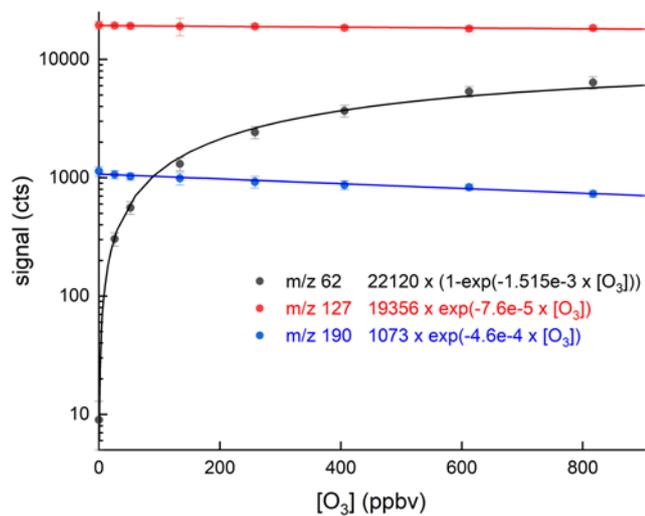
**Figure 8**. Dependence of the signals at *m/z* 62 and *m/z* 190 on the $O_3$ mixing ratio with $HNO_3$ fixed at 12.5 ppbv. The lines through the data are described by the expressions listed in the Figure.

625
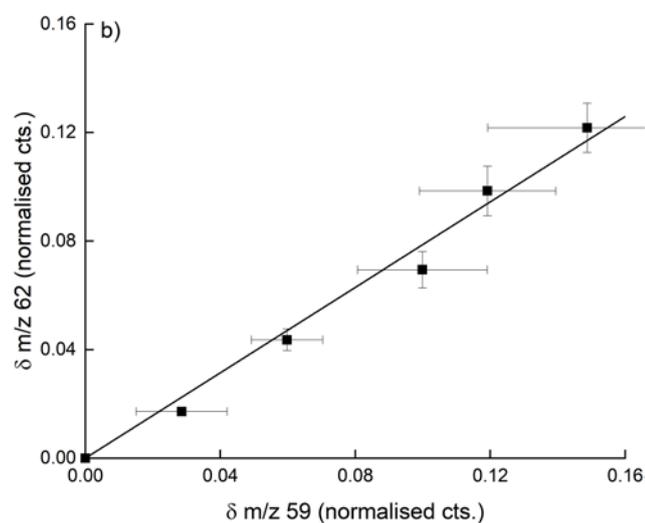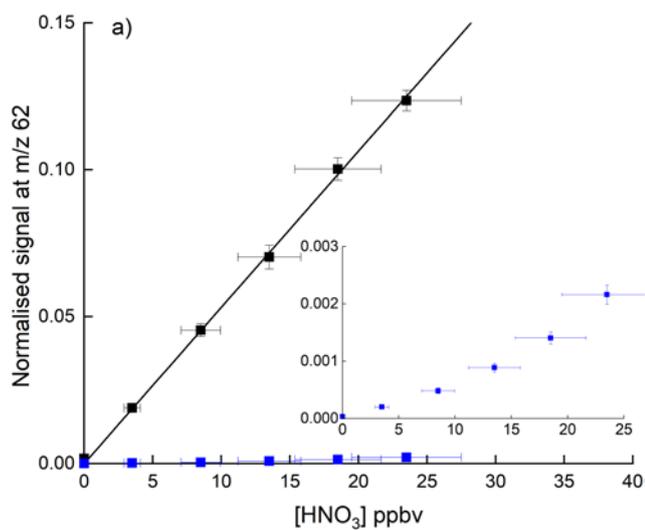
630 **Figure 9**. a) Detection of $HNO_3$ at *m/z* 62 in the presence of 3.25 ppbv PAA (and thus the acetate anion, $CH_3CO_2$). The blue data points (expanded view in the inset) were obtained in the absence of PAA, whereby detection of $HNO_3$ at *m/z* 62 is inefficient. The error bars are 1σ statistical uncertainty in the signal at *m/z* 62 and 17 % total uncertainty in the $HNO_3$ mixing ratio. (b) Change in normalised signals at *m/z* 62 and *m/z* 59 upon adding $HNO_3$ for the same dataset (i.e. background corrected signals). The error bars are 1σ statistical uncertainty.

635
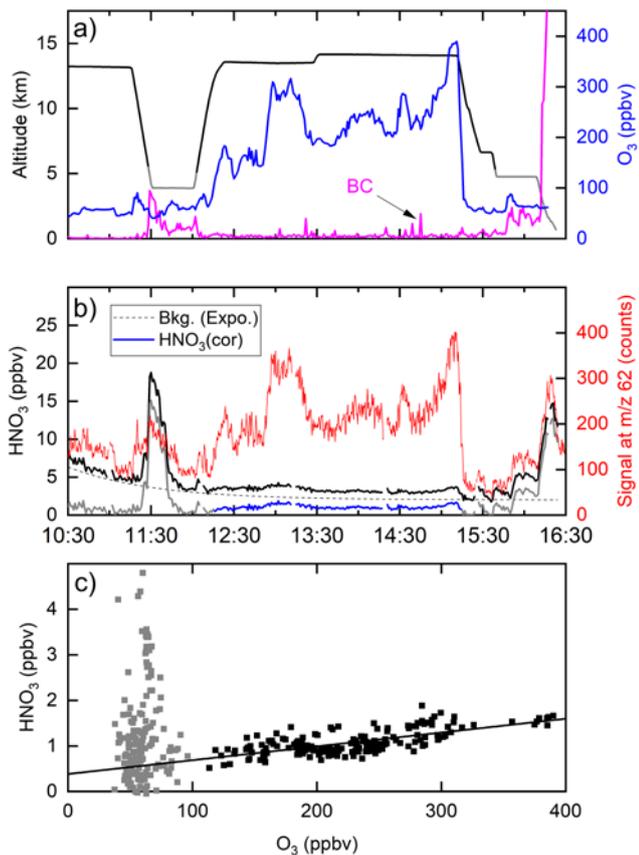
**Figure 10.** a) Altitude (black) and $O_3$ mixing ratios (blue) from a HALO-flight during the CAFE-Africa campaign. The purple line (arbitrary units) is proportional to the black-carbon particle number density (BC). b) The signal at $m/z$ 62 (red line) clearly co-varies with $O_3$. Following conversion to a mixing ratio (black line) and subtraction of an $HNO_3$ background signal (dotted line, assuming an exponential decay) originating in the $^{210}$Po-source, the solid blue line for $HNO_3$ is obtained ($HNO_3$ cor). c) $HNO_3$ mixing ratios plotted versus $O_3$ mixing ratios. The straight black line has a slope of $(3 \pm 0.5) \times 10^{-3}$ and does not take into account the grey data points ($O_3$ mixing ratio < 100 ppbv).

645
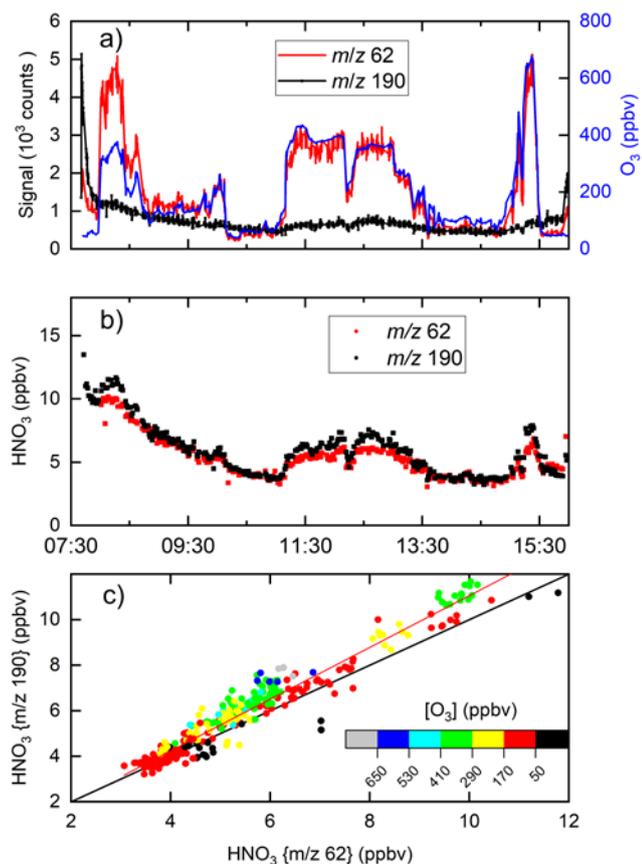
**Figure 11**. I-CIMS HNO₃ measurements and auxiliary data from a HALO-flight during the CAFE-EU campaign. a) Signals at $m/z$ 62 and $m/z$ 190 as well as O₃ mixing ratios. b) HNO₃ mixing ratios derived from the signals at $m/z$ 62 and $m/z$ 190 taking the dependence of sensitivity on ozone and relative humidity into account. c) Correlation of the HNO₃ mixing ratios derived from the two masses. The red line is a bivariate fit (slope 1.14 ± 0.05, intercept -0.3 ± 0.3), the black line is a 1:1 line. A large fraction of the HNO₃ measured stems from the polonium source, especially at the beginning of the flight.